

# Renormalization Group Flow Equation at Finite Density

J. Meyer<sup>1</sup>, G. Papp<sup>1,2,\*</sup>, H.-J. Pirner<sup>1,3</sup> and T. Kunihiro<sup>4</sup>

<sup>1</sup> Institut für Theoretische Physik der Universität Heidelberg,  
D-69120 Heidelberg, Germany

<sup>2</sup> CNR, Department of Physics, Kent State University, 44242 OH USA

<sup>3</sup> Max-Planck-Institut für Kernphysik, D-69029 Heidelberg, Germany

<sup>4</sup> Faculty of Science and Technology, Ryukoku University, Seta, Ohtsu 520-2194, Japan

November 16, 2018

## Abstract

For the linear sigma model with quarks we derive renormalization group flow equations for finite temperature and finite baryon density using the heat kernel cutoff. At zero temperature we evolve the effective potential to the Fermi momentum and compare the solutions of the full evolution equation with those in the mean field approximation. We find a first order phase transition either from a massive constituent quark phase to a mixed phase, where both massive and massless quarks are present, or from a metastable constituent quark phase at low density to a stable massless quark phase at high density. In the latter solution, the formation of droplets of massless quarks is realized even at low density.

PACS: 12.39.Fe; 11.10.Hi; 21.65.+f

---

\*On leave from HAS Research Group for Theoretical Physics, Eötvös University, Pázmány P. s. 1/A, Budapest, H-1117 Hungary

# 1 Introduction

Recently a transparent approach to the evolution of a hadronic system with resolution has been constructed using a Schwinger proper time representation of the fluctuation determinants of quarks and chiral mesons [1]. This method gives a picture of the transformation of constituent quarks at low resolution into partonic massless quarks at high resolution observed in deep inelastic scattering [2]. At finite temperature the same type of renormalization group (RG) flow equations give critical indices for the chiral phase transition in agreement with the  $O(4)$  model [1, 3]. Present finite temperature QCD lattice simulations seem to indicate such an  $O(4)$  type behavior, with some uncertainty.

Simulation of QCD at finite baryon density on a lattice is still a challenge: In Euclidean space the chemical potential gives rise to a complex action which forbids Monte Carlo calculations. Quenched simulations at finite density suffer from additional shortcomings [4]. The challenge is therefore to come up with a calculational scheme for finite baryon density which has a well controlled predictive power. Theoretical studies of high density matter given in this work are indispensable to understand what is going on with high-energy heavy ion collisions which probe not only high excitation energy (perhaps temperature) but also high baryonic density. Recent studies have suggested a very rich phase structure at high baryon density [5, 6]. There has been considerable work devoted to extract the equation of state of nuclear matter in terms of nucleon - nucleon potentials. The problem is to link the high density region accessed by high energy heavy ion collisions with the low density nuclear physics region.

At low density it is probably not very efficient to describe baryonic matter by quarks, but in an intermediate region, quarks and mesonic bound states may be the right degrees of freedom. The mesons are formed by the strong gluonic attraction in certain channels. The chiral linear sigma model with quarks is a good model to investigate the dynamics below a momentum scale of  $k < k_{uv} = 1.2 \text{ GeV}^1$ . Such a hybrid approach has been already used at finite temperature with success. In this paper we will treat pure quark matter and concentrate on chiral symmetry aspects of the transition. We neglect quark confinement but assume the gluons to be confined into the mesons.

---

<sup>1</sup>The definition of this momentum scale depends on the renormalization group scheme.

The connection to nuclear matter will be considered elsewhere [7]. The finite baryon density dynamics is much more sensitive to neglecting confinement than the finite temperature dynamics. Indeed it is known that e.g. the *NJL* model gives a first order phase transition at unrealistically low baryon density [8, 9]. Without confining quark forces, which repel quarks tripled in neutral nucleons from each other [10], the linear sigma model with quarks probably overestimates the binding energy per baryon of nuclear matter.

We use renormalization group flow equations in the presence of finite quark density. As a first step, we start with the heat kernel representation of the effective potential using the cut-off function of the earlier finite temperature calculation [1]. The extension of this technique to finite density is straightforward in contrary to the cut-off function introduced by the Wetterich group [11] for finite temperature studies. However, the proposed method has its shortcomings: **1.** The heat kernel cutoff is a Lorentz invariant cutoff, and as such does not zoom to the Fermi surface with increasing evolution steps. In principle the goal of the renormalization group approach for finite fermion density is [12] to treat the critical long wave length particle hole excitations of the finite Fermi system towards the end of the evolution. These particle hole excitations are generated at the Fermi surface. In the relativistic case with Goldstone bosons this final evolution step should coincide with the treatment of the zero mass bosons. **2.** Extra terms which reduce the ultraviolet sensitivity in our heat kernel cut-off function result in an integration pole at the Fermi surface, making the numerical integration difficult.

In this paper we concentrate on deriving the formalism for a finite density calculation with finite temperature. We solve the flow equations for finite density at temperature  $T = 0$  leaving our final goal, the determination of the phase diagram in the whole  $(T, \mu)$  plane to another paper. Furthermore, we compare our renormalization group results with the mean field approximation.

As a description of choice in this work we use the linear sigma model. We think that this model can play the role of a simplified theory showing the effects of relativistic field theory at finite density as a kind of Ising model for nuclear physics. The equation of state improved by the renormalization group in the one loop gives clear signals on what is happening in the finite density system. The main message is the intricate connection between the effective mass of the fermions and the effective masses of the mesons ex-

changed between the fermions. In classical nonrelativistic nuclear physics the time scale of the meson exchange is short in comparison with the time scale of the nucleon dynamics. At normal nuclear density the mesons will not be modified drastically by the nuclear medium. In the quark picture the time scale for the exchange of a meson is not different from the time scale connected to the rearrangement of the fermion momenta. The mesons cannot be taken into account as potentials, which are turned into effective interactions, due to the quark rescattering in the medium. The mesons participate fully in the reorganization of the chiral symmetric phase with increasing density. The quark many body problem is therefore very different from the nuclear physics problem where the nucleon dynamics largely decouples from the meson dynamics. The only possible tool we have to solve such an intrinsically nonlinear problem in field theory is the renormalization group, therefore it is worth to study this technique in nuclear physics to get a better understanding of the phase structure of baryonic matter.

The paper is organized as follows: in section 2 we review the derivation of the renormalization group flow equation for the effective potential at zero density and temperature. The extension of this method to finite temperature and baryon density is presented in section 3. At the end of this section we show a first result from the RG flow equation at finite density. In section 4 we discuss the mean field approximation to the linear sigma model and in section 5 we present our results for two sets of mean field couplings, obtained from the RG evolution. Here we study the finite baryon density phase transition of the linear sigma model in the mean field approximation. In section 6 we compare the results of the grid and the mean field calculations. Section 7 is devoted to a summary and to the conclusions. In the Appendices we discuss the connection between the fermionic part of the flow-equations and the mean field result and give a detailed derivation of the flow equations at finite temperature and density.

## 2 Evolution of the linear $\sigma$ model

We consider the chiral constituent quark model with quarks,  $\sigma$  and  $\pi$  mesons. At zero temperature and chemical potential in Euclidean space the partition

function or the generating functional without external sources  $\Delta$ , is given by

$$Z[\Delta = 0] = \int \mathcal{D}q \mathcal{D}\bar{q} \mathcal{D}\sigma \mathcal{D}\vec{\pi} \exp\left\{-\int d^4x (\mathcal{L}_F + \mathcal{L}_B)\right\} \quad (1)$$

with a fermionic  $\mathcal{L}_F$ , and a bosonic  $\mathcal{L}_B$ , parts,

$$\mathcal{L}_F = \bar{q}(x) [\gamma_E \partial_E + g(\sigma + i\vec{\tau}\vec{\pi}\gamma_5)] q(x), \quad (2)$$

$$\mathcal{L}_B = \frac{1}{2} [(\partial_\mu \sigma)^2 + (\partial_\mu \vec{\pi})^2] + F(\sigma^2 + \vec{\pi}^2). \quad (3)$$

The Yukawa coupling of the constituent quarks to the mesons is denoted by  $g$ . The parameters of the linear  $\sigma$ -model at  $T = 0$  are chosen in the same way as in ref. [1, 3]. We assume that at an ultraviolet scale  $k_{uv}$ , the full  $QCD$  dynamics reduces to a hybrid description in terms of quarks and chiral bound states. The gluons are assumed to be frozen in the residual mesonic degrees of freedom and their couplings.

At the beginning of the evolution at  $k_{uv} = 1.2$  GeV we choose the effective potential density  $F_0$ , to be of the following form:

$$F_0(\vec{\phi}) = \frac{m^2}{2} \phi^2 + \frac{\lambda}{4} \phi^4, \quad \text{with } \phi^2 = \sigma^2 + \vec{\pi}^2, \quad (4)$$

where the positive mass squared  $m^2 = 0.4^2$  GeV<sup>2</sup> reflects a symmetric ground state, i.e. the minimum of the potential lies at the origin. The four boson coupling at this scale is  $\lambda = 30$  [1, 3]. The values correspond to a critical temperature  $T_c \approx 150$  MeV, and a chiral symmetry breaking scale  $k_{br} \approx 1$  GeV which one obtains after performing the RG procedure.

The effective potential density  $F(\phi)$ , can be evolved [1] using the heat kernel method. For this purpose the one loop effective potential is calculated with a cutoff function  $f(k^2\tau)$ , which contains the evolution scale  $k$ :

$$f(x = k^2\tau) = e^{-x} \left(1 + x + \frac{1}{2}x^2\right). \quad (5)$$

Doing this, the couplings of the of the effective potential become scale dependent:  $m = m(k)$  and  $\lambda = \lambda(k)$ .

Using the the Schwinger proper time representation the fermionic  $F^F$  contribution to the effective potential density is:

$$\begin{aligned} F^F &= \frac{1}{2} \int_0^\infty \frac{d\tau}{\tau} f(k^2\tau) \int \frac{d^4q}{(2\pi)^4} \text{Tr} e^{-\tau[q^2+g^2\phi^2]} \\ &= \frac{1}{2} 4N_c N_f \int_0^\infty \frac{d\tau}{\tau} f(k^2\tau) \int \frac{d^4q}{(2\pi)^4} e^{-\tau[q^2+g^2\phi^2]} \end{aligned} \quad (6)$$

and correspondingly [1] the bosonic part is:

$$\begin{aligned} F^B &= -\frac{1}{2} \int_0^\infty \frac{d\tau}{\tau} f(k^2\tau) \int \frac{d^4q}{(2\pi)^4} \text{Tr} e^{-\tau[q^2+\frac{\partial^2 F_0}{\partial\phi_i\partial\phi_j}]} \\ &= -\frac{1}{2} \int_0^\infty \frac{d\tau}{\tau} f(k^2\tau) \int \frac{d^4q}{(2\pi)^4} e^{-\tau[q^2]} [3e^{-\tau 2F'_0} + e^{-\tau[2F'_0+4F''_0\phi^2]}], \end{aligned} \quad (7)$$

with

$$F_0 = F_0(\phi^2, k), \quad F'_0 = \frac{\partial F_0}{\partial\phi^2}, \quad F''_0 = \frac{\partial^2 F_0}{(\partial\phi^2)^2}. \quad (8)$$

The total effective potential density is the sum of these two terms,  $F = F^B + F^F$ . The evolution equation of this potential results from the derivative of the potential with respect to  $k$ . In the spirit of the renormalization group improved 1-loop approximation the derivative only acts on the cutoff function and the potential density  $F_0$ , is replaced by the evolving potential density  $F$ . The evolution equation for the linear sigma model then has the following simple form:

$$\frac{\partial F}{\partial k} = \frac{k^5}{32\pi^2} \left\{ \frac{3}{k^2+2F'} + \frac{1}{k^2+2F'+4F''\phi^2} - \frac{8N_c}{k^2+g^2\phi^2} \right\}. \quad (9)$$

In the approximation to the RG-evolution used here only the effective potential density  $F$ , evolves with the scale  $k$ . The Yukawa-coupling  $g = 3.23$  is assumed to be constant. The limitation of this approach will be discussed later. Note that during the evolution one passes from the region with  $m^2 > 0$ , where the potential is symmetric, to the region  $m^2 < 0$  where the potential has a mexican hat shape. The denominators of the meson loop terms (e.g. the first two terms on the l.h.s. of eq. (9)) indicate a limitation of the one

loop renormalization flow. The one loop corrections are of order  $\mathcal{O}(\hbar)$  in an expansion in  $\hbar$ . In the regime  $k^2 + 2F' \leq 0$  however, the usual Gaussian fixed point is unstable and a non-Gaussian fixed point should be considered bringing in  $\mathcal{O}(\hbar^0)$  effects [13]. With our choice of parameters this happens at  $k \leq k_{inst} \approx 200$  MeV.

### 3 Evolution equation at finite density

The renormalization group flow equations give a well determined shape of the effective potential with which we will work in this section. Since they are formulated in the continuum, the finite baryon density  $\rho_B$  can be implemented. Although the primary aim of the present work is to discuss the chiral transition at finite baryonic density, we shall present the master formulae for finite temperature  $T$  and finite  $\rho_B$  and then take the limit  $T \rightarrow 0$ .

We start our derivation from eqs. (6,7) extending them to finite temperature and finite chemical potential. Since we are working now with fixed temperature and chemical potential, one should replace the potential density  $F$ , by the thermodynamical potential density  $\Omega(\phi^2)$ . The fermionic part of the effective potential density generalized to finite temperature  $T$  and chemical potential  $\mu$  is

$$\Omega^F = \frac{T}{2} 4N_c N_f \int_0^\infty \frac{d\tau}{\tau} f(k^2\tau) \sum_n \int \frac{d^3q}{(2\pi)^3} e^{-\tau[(\nu_n + i\mu)^2 + \vec{q}^2 + g^2\phi^2]}, \quad (10)$$

with the cutoff function  $f(x)$  given by eq. (5), and the Matsubara frequencies  $\nu_n = (2n + 1)\pi T$  for fermions. The bosonic part is the one already examined in [1],

$$\Omega^B = -\frac{T}{2} \int_0^\infty \frac{d\tau}{\tau} f(k^2\tau) \sum_n \int \frac{d^3q}{(2\pi)^3} e^{-\tau(\omega_n^2 + \vec{q}^2)} [3e^{-\tau 2\Omega'_0} + e^{-\tau(2\Omega'_0 + 4\Omega''_0\phi^2)}] \quad (11)$$

with Matsubara frequencies  $\omega_n = 2n\pi T$  for bosons. The derivatives in the potential are taken again with respect to  $\phi^2$ . The total effective potential density is the sum of the two terms,  $\Omega = \Omega^B + \Omega^F$ .

An advantage of the heat kernel regulator is that the calculation of derivatives with respect to the momentum scale  $k$  can be performed analytically

to yield compact formulae. As shown in appendix A, we have

$$\frac{\partial\Omega^F}{\partial k^2} = \frac{N_c N_f}{8\pi^2} k^4 \frac{d}{dk^2} \int_0^\infty dq \frac{1}{E_{q,k}} [1 - n(E_{q,k}) - \bar{n}(E_{q,k})], \quad (12)$$

where  $E_{q,k} = \sqrt{q^2 + k^2 + g^2\phi^2}$  and  $n(x)$  and  $\bar{n}(x)$  are the Fermi-Dirac distribution functions for particles and anti-particles. Evaluating the derivative with respect to  $k^2$  on the right hand side, we obtain

$$\begin{aligned} \frac{\partial\Omega^F}{\partial k^2} = & -\frac{N_c N_f}{32\pi^2} k^4 \int_0^\infty dq \left[ \frac{1}{E_{q,k}^3} (1 - n(E_{q,k}) - \bar{n}(E_{q,k})) \right. \\ & \left. - \frac{1}{TE_{q,k}^2} \{n(E_{q,k})(1 - n(E_{q,k})) + \bar{n}(E_{q,k})(1 - \bar{n}(E_{q,k}))\} \right]. \quad (13) \end{aligned}$$

We notice that the distribution functions explicitly show how the temperature and the baryonic density modify the  $T = 0$  and  $\rho_B = 0$  result: The right hand side of the evolution equations in vacuum is diminished (1) by the Pauli blocking effect as seen in the first bracket, and (2) by the thermally excited states as seen in the second bracket. Similarly, the bosonic part at  $T \neq 0$  is evaluated as shown in appendix A, where  $\partial\Omega^B/\partial k^2$  is expressed in terms of the Bose-Einstein distribution function.

Although formula (13) is generally valid for  $T \neq 0$  and  $\rho_B \neq 0$ , it is not useful when the temperature is set to zero due to the factor  $T^{-1}$  in the second bracket. The zero temperature formula is obtained easily from eq. (12) making the substitutions  $n(E_{q,k}) \rightarrow \theta(\mu - E_{q,k})$  and  $\bar{n}(E_{q,k}) \rightarrow 0$ :

$$\left. \frac{\partial\Omega^F}{\partial k} \right|_\mu = -\frac{N_c N_f}{8\pi^2} \frac{k^5}{k^2 + g^2\phi^2} \left[ 1 - \frac{\mu}{\sqrt{\mu^2 - k^2 - g^2\phi^2}} \Theta(\mu - \sqrt{k^2 + g^2\phi^2}) \right]. \quad (14)$$

Here again we see how the evolution equation at finite baryon density is modified by Pauli blocking. In appendix B we show how the integral of the finite density part of equation (14) gives the mean field result, which will be presented in section 4.

For the charge neutral system (zero bosonic chemical potential) at  $T = 0$  the bosonic term is the same as in vacuum. Adding both contributions, we have the zero temperature flow equation for finite baryon density as follows:

$$\left. \frac{\partial\Omega}{\partial k} \right|_\mu = \frac{k^5}{32\pi^2} \left\{ \frac{3}{k^2 + 2\Omega'} + \frac{1}{k^2 + 2\Omega' + 4\Omega''\phi^2} \right\} \quad (15)$$



$$-\frac{4N_c N_f}{k^2 + g^2 \phi^2} \left( 1 - \frac{\mu}{\sqrt{\mu^2 - k^2 - g^2 \phi^2}} \Theta(\mu - \sqrt{k^2 + g^2 \phi^2}) \right) \Bigg\}.$$

We stress that such a compact form is obtained for the flow equation in the heat-kernel method; the Pauli blocking effect due to the presence of the Fermi sea is explicitly represented by a theta-function. This is certainly an advantage of the method. However, the presence of the theta-function makes numerical evaluations difficult because its derivatives produce singular terms which are not easy to control in the numerical analysis.

As an attempt to circumvent this difficulty, we let the chemical potential run during the evolution; so the chemical potential will be a function of the scalar field and the momentum scale  $\mu = \mu(\phi, k)$ , as proposed by Shankar in reference [14]. In fact, it turns out that no singularities of the fermion-terms appear in the evolution with a running  $\mu$ . In the functional integral for  $\Omega$  we explicitly insert a  $k$ -dependent chemical potential.

The method is best explained starting from  $k = 0$ . At the end of the evolution the transition to the free energy density can be made via a Legendre transformation.

$$F(k=0, \phi^2) = \Omega(k=0, \phi^2) + \rho \mu(k=0, \phi^2), \quad (16)$$

where  $\mu(k=0)$  has to be eliminated from  $\Omega(k=0, \phi^2)$  via the equation

$$\frac{\partial \Omega(k=0)}{\partial \mu(k=0)} = -\rho. \quad (17)$$

Now we make a small change of infrared cut-off scale  $k$  and adjust  $\mu(k)$  in such a way that the density remains constant:

$$\frac{\partial \Omega}{\partial \mu(k)} = -\frac{\partial \Omega^F}{\partial \mu(k)} = -\rho. \quad (18)$$

The same procedure is repeated at each step of  $k$ . The explicit evaluation of the l.h.s. at a finite evolution scale  $k$  using (10) yields

$$\rho = \frac{2N_c}{3\pi^2} \left( x_F^3 + \frac{3}{2} k^2 x_F + \frac{3}{8} \frac{k^4}{x_F} \right), \quad (19)$$

with

$$x_F = \sqrt{\mu^2 - k^2 - g^2 \phi^2}. \quad (20)$$

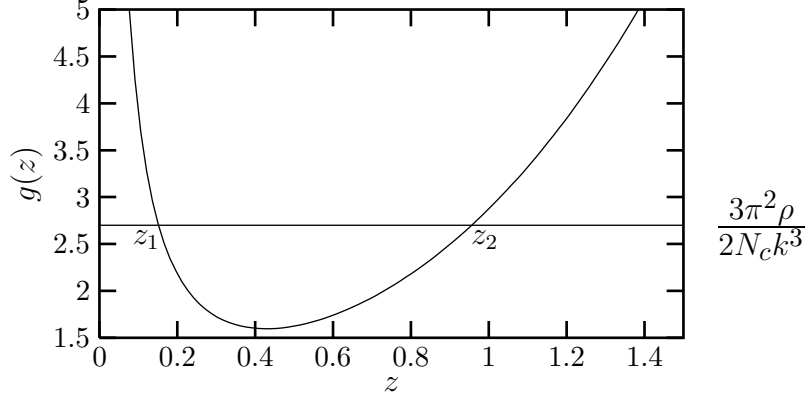


Figure 1: The function  $g(z)$  with  $z = x_F/k$ , which allows to find the solutions of the constraint eq. (22) at a fixed density  $\rho$ .

An analysis of the solutions  $\mu(x_F)$  from eq. (19) shows that at  $k = 0$  this equation has a unique solution  $\mu = \sqrt{g^2 \phi^2 + k_F^2}$ , with the Fermi momentum  $k_F$  defined by  $\rho = 2N_c k_F^3 / 3\pi^2$ . For  $k \neq 0$  it is advantageous to discuss the solutions in terms of  $z = x_F/k$ . Equation (19) then reads

$$\rho = \frac{2N_c}{3\pi^2} k^3 \cdot g(z), \quad (21)$$

with

$$g(z) = z^3 + \frac{3}{2}z + \frac{3}{8z}. \quad (22)$$

The behavior of  $g(z)$  is shown in Figure 1;  $g(z)$  has the minimum

$$g_{min} = \frac{1}{2} \frac{\sqrt{3} + 1}{\sqrt{\sqrt{3} - 1}} \quad (23)$$

at  $z = \frac{1}{2}\sqrt{\sqrt{3} - 1} \equiv z_m$ . At finite evolution scale  $k$  the line of constant  $\frac{3\pi^2\rho}{2N_c k^3}$  will in general cut the constraint function at two points  $z_1$  and  $z_2$ . It is necessary for the equation to have real solutions that

$$k \leq \left( \frac{3\pi^2\rho}{N_c} \frac{\sqrt{\sqrt{3}-1}}{\sqrt{3}+1} \right)^{1/3} \equiv k_{th}. \quad (24)$$

At  $k = k_{\text{th}}$  the line of constant  $\frac{3\pi^2\rho}{2N_c k^3}$  is tangential to  $g(z)$  at  $z = z_m$ . Corresponding to the two solutions, the chemical potential has two different values at fixed density:

$$\mu_i(k) = \sqrt{k^2 z_i(k)^2 + k^2 + g^2 \phi^2} \quad (i = 1, 2). \quad (25)$$

The derivatives  $\partial\mu_i/\partial k$  are calculated by demanding that the baryon density found at  $k = 0$  remains the same *independently* of the evolution scale  $k$ . Thus the  $k$  derivative of the l.h.s of eq. (19) is zero, leading to

$$\frac{\partial\mu_i}{\partial k} = -\frac{1}{\mu_i} \frac{k}{8z_i^4 + 4z_i^2 - 1}. \quad (26)$$

Applying the chain rule one can calculate the flow equation for the thermodynamic potential with running chemical potential,

$$\frac{\partial\Omega}{\partial k} \Big|_{\mu(k)} = \frac{\partial\Omega}{\partial k} \Big|_{\mu=\text{const.}} + \frac{\partial\Omega}{\partial\mu} \frac{\partial\mu(k)}{\partial k} = \frac{\partial\Omega}{\partial k} \Big|_{\mu=\text{const.}} - \rho \frac{\partial\mu(k)}{\partial k}, \quad (27)$$

or rearranging this formula for each  $k$  we get the equivalent free energy at each  $k$ :

$$\frac{\partial F}{\partial k} \Big|_{\rho_B} = \frac{\partial(\Omega + \rho\mu)}{\partial k} \Big|_{\mu(k)} = \frac{\partial\Omega}{\partial k} \Big|_{\mu=\text{const.}}. \quad (28)$$

We can eliminate the chemical potential in the flow-equation at each  $k$  via a  $\delta$ -function,

$$1 = \int df \delta[f(z)], \quad (29)$$

with

$$f(z) = \frac{2N_c}{3\pi^2} k^3 g(z) - \rho. \quad (30)$$

The evolution equation (27) with running chemical potential has two terms  $i = 1, 2$  corresponding to the two roots of the constraint equation:

$$\frac{\partial\Omega}{\partial k} \Big|_{\mu(k)} = \int df \delta[f(z)] \left[ \frac{\partial\Omega}{\partial k} \Big|_{\mu=\text{const.}} + \frac{\partial\Omega}{\partial\mu} \frac{\partial\mu(k)}{\partial k} \right] \quad (31)$$

$$= \sum_{i=1,2} \int \frac{\partial f}{\partial z} dz \left| \frac{\partial f}{\partial z} \right|^{-1} \delta(z - z_i) \left[ \frac{\partial\Omega}{\partial k} \Big|_{\mu=\text{const.}} - \rho \frac{\partial\mu(k)}{\partial k} \right]. \quad (32)$$

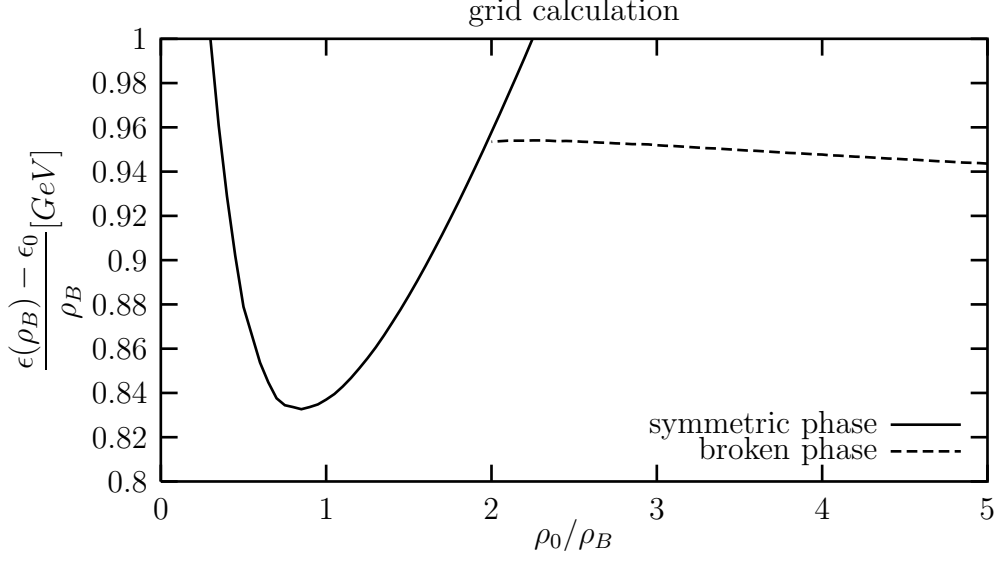


Figure 2: Normalized energy per baryon plotted against inverse density  $\rho_B^{-1}$ , normalized to normal nuclear density  $\rho_0 = 0.16 \text{ fm}^{-3}$ , in the broken phase (dashed line) and in the symmetric phase (solid line). The evolution eq. (33) is solved on the grid. The energy of the broken phase at zero density is  $\epsilon_0$ .

Note that at the two zeros of the function  $f$ ,  $z_1$  and  $z_2$ , the Jacobians have opposite signs (see figure 1) leading to some cancellation. Thus we arrive at the final flow equation

$$\begin{aligned} \frac{\partial \Omega}{\partial k} \Big|_{\mu(k)} &= \frac{k^5}{32\pi^2} \left\{ \frac{3}{k^2 + 2\Omega'} + \frac{1}{k^2 + 2\Omega' + 4\Omega''\phi^2} - \frac{8N_c}{k^2 + g^2\phi^2} \right\} \\ &+ \sum_{i=1,2} (-1)^i \left\{ \frac{N_c}{4\pi^2} \frac{k^4}{k^2 + g^2\phi^2} \frac{\mu_i}{z_i} + \frac{\rho}{\mu_i} \frac{k}{8z_i^4 + 4z_i^2 - 1} \right\} \Theta(k_{\text{th}} - k). \end{aligned} \quad (33)$$

The reason of the presence of the theta-function in (33) is apparent from (10). Note that the term  $1/(8z_i^4 + 4z_i^2 - 1)$  is singular at  $k = k_{\text{th}}$  but can be integrated analytically.

Equation (33) is the evolution equation with running chemical potential  $\mu(k)$  at zero temperature for the thermodynamic potential density. In order

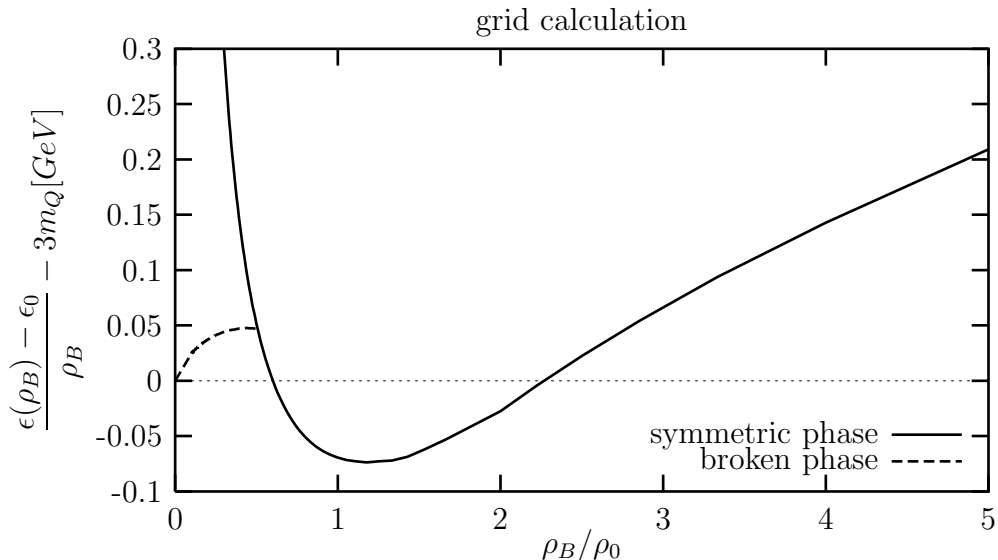


Figure 3: The binding-energy per baryon calculated from the evolution equation on the grid is shown as a function of  $\rho_B$  normalized to normal nuclear density  $\rho_0$ .

to follow the minimum of the order parameter at fixed density we need the free energy density. Recall that at  $k = 0$  there is only one solution to the constraint equation (19) which is related to  $z_2$ , therefore we can calculate the free energy density  $F$  at  $k = 0$  from the thermodynamic potential density  $\Omega(k = 0)$  and the chemical potential  $\mu(k = 0)$ :

$$\begin{aligned}
 F(k=0, \phi^2) &= \Omega(k=0, \phi^2) + \rho\mu(k=0, \phi^2) \\
 \mu(k=0, \phi^2) &= \sqrt{k_F^2 + g^2\phi^2}
 \end{aligned}
 \tag{34}$$

Due to the theta term in eq. (33) the  $k$  evolution of  $\Omega(k)$  and  $F(k)$  is the same till  $k_{th}$  and does not feel the baryon density. Below  $k_{th}$  the density effects set in with the contributions of a shell of fermions. During the course of evolution the outside radius of the shell increases and the inside radius diminishes until the longest wavelengths in the fermi sea are integrated. The effect arising from the fermi sea is classical, hence  $\mathcal{O}(\hbar^0)$  and dominates the RG flow equation. For large enough densities  $\rho \gtrsim 0.45\rho_0$ , we have  $k_{th} > k_{inst}$

and eq. (9) is replaced by the density driven evolution without unstable boson terms.

We solved eq. (33) numerically on a grid: the full potential density  $\Omega$ , is discretized as a function of  $\phi^2$  on a grid of hundred points between  $0 < \phi^2 < 0.05 \text{ GeV}^2$ . The resulting hundred differential equations are solved with a Runge Kutta method.

As we discussed earlier at the end of section 2 the meson terms in the flow equation (33) develop singularities due to the instability of the effective potential. This behavior is well known in the literature [15, 16], the mesonic effective potential in the one loop approximation generates tachyonic meson masses. The renormalization group scale  $k^2$  avoids these poles for some part of the evolution, but cannot get rid of them totally. The singularities in the boson denominators of the evolution equation appear at  $k_{inst}^2 + 2\Omega' = 0$ , indicating the disappearance of the Gaussian fix point [13]. As our studies show the inclusion of the non-Gaussian fixed point does not change the position of the minimum considerably at zero temperature. Hence in this paper we neglect the singular mesonic contributions beyond  $k = k_{inst}$  in the evolution equation leaving the more exact solution to a future work. The results of the grid calculation are shown in figures 2 and 3. We will discuss them extensively in section 6 and compare them with the mean field calculations presented in the next section.

## 4 Coarse grained potential in mean field approximation

Since the numerical solution of the RG flow equations has difficulties at small momentum scale  $k$ , we discuss another approximation to the low momentum region in this section. We evolve the vacuum theory from the ultraviolet scale  $k = k_{uv}$  down to  $k = k_F$  corresponding to normal nuclear matter density  $\rho_B = \rho_0$ . Thereby we obtain a coarse grained potential which is appropriate for the dynamics at these low momenta. This potential contains the vacuum loop effects of the quarks and bosons integrated out up to this scale. Then we solve this coarse grained linear sigma model in mean field approximation.

To keep the mean field approximation transparent we approximate the coarse grained potential with the original fourth order form of equation (4)

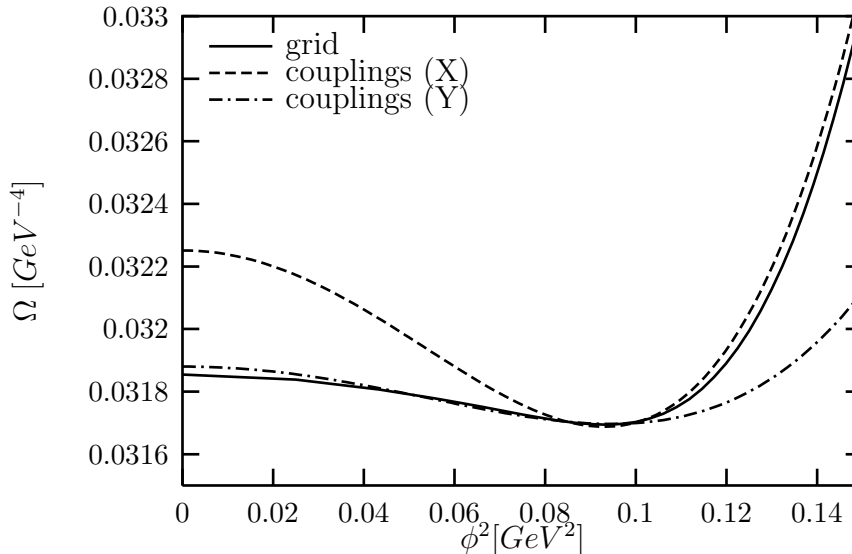


Figure 4: The potential  $\Omega(\phi^2)$  at momentum scale  $k = k_{th}$ , from the grid calculation (solid line) and the fitted curves with mean field parameters  $X$  (dashes) and  $Y$  (dashed-dotted line). See table 1.

with renormalized parameters. These parameters depend on the range in  $\phi^2$  where the fit to the coarse grained potential is done. We have chosen two sets: a fit on a wider region in  $\phi^2$  ( $X$ ) and a narrower one ( $Y$ ). The resulting parameters are summarized in Table 1. The coarse grained potential and the two fits are shown in figure 4. The negative values of the mass squared indicate that at the scale  $k = k_F$  we already entered the broken phase, with a nonvanishing expectation value of the  $\sigma$  field,  $\bar{\sigma}$ . A mean field solution with these potentials is straightforward by evaluating the Hamiltonian  $H$ , in the presence of the Fermi sea and then minimizing  $H$  with respect to  $\bar{\sigma}$ . Since we have already taken into account quantum fluctuations from the Dirac sea and the bosons in the evolution, we do not need to consider these pure quantum fluctuations any longer. Their effects are assumed to be of higher scale than  $k_F$  and therefore they are integrated up in the coarse grained potential. Of course, we are missing typical quantum many body fluctuations not included in the mean field approximation of the many body system.

Type	Fit range $\phi^2$	$m_{MF}^2$	$\lambda_{MF}$	$\bar{\sigma}_0$	$3g\bar{\sigma}_0$	$B^{1/4}$	$m_\sigma$
X	[0, 0.05]	-0.260	30.0	0.0940	0.902	0.15554	0.720
Y	[0, 0.01]	-0.082	9.18	0.0945	0.906	0.11633	0.405
grid	-	-	-	0.0944	0.906	-	-

Table 1: Effective meson potentials used. The fit range and the mass parameter  $m_{MF}^2$  are in  $\text{GeV}^2$ , the  $\bar{\sigma}_0$ ,  $B^{1/4}$  and the mass of the  $\sigma$  meson are in GeV.

The mean field solution of the resulting  $\phi^4$  theory is standard. The Hamiltonian reads

$$H = \int d^3x \left[ q^\dagger (\vec{\alpha}\vec{p} + g\beta\bar{\sigma}) q + \frac{m_{MF}^2}{2}\bar{\sigma}^2 + \frac{\lambda_{MF}}{4}\bar{\sigma}^4 \right]. \quad (35)$$

Using a plane-wave basis for the quarks one can rewrite the Hamiltonian as an integral over momenta. In the ground-state,  $T = 0$ , the Fermi-sphere is filled from the bottom up to the Fermi-momentum  $k_F$ . The energy density is evaluated to be

$$\begin{aligned} \epsilon = \frac{E}{V} &= \frac{4N_c}{(2\pi)^3} \int_0^{k_F} d^3k \sqrt{k^2 + g^2\bar{\sigma}^2} + \frac{1}{2}m_{MF}^2\bar{\sigma}^2 + \frac{\lambda_{MF}}{4}\bar{\sigma}^4 \quad (36) \\ &= \frac{N_c}{4\pi^2} \left( 2k_F\sqrt{k_F^2 + g^2\bar{\sigma}^2}^3 - g^2\bar{\sigma}^2 k_F\sqrt{k_F^2 + g^2\bar{\sigma}^2} \right. \\ &\quad \left. - g^4\bar{\sigma}^4 \log \frac{\sqrt{k_F^2 + g^2\bar{\sigma}^2} + k_F}{g\bar{\sigma}} \right) + \frac{1}{2}m_{MF}^2\bar{\sigma}^2 + \frac{\lambda_{MF}}{4}\bar{\sigma}^4. \end{aligned}$$

The quark Fermi-momentum is fixed by the quark-density  $\rho = 3\rho_B$ ,

$$k_F = \sqrt[3]{\frac{3\pi^2\rho}{2N_C}}. \quad (37)$$

The mean  $\sigma$ -field configuration is calculated by minimizing (36) with respect to  $\bar{\sigma}$ . One ends up with a self-consistent equation for the mean field



$\bar{\sigma}$ ,

$$\left(\frac{\partial \epsilon}{\partial \bar{\sigma}}\right)_V = \frac{4N_c}{(2\pi)^3} \int_0^{k_F} d^3k \frac{g^2 \bar{\sigma}}{\sqrt{k^2 + g^2 \bar{\sigma}^2}} + m_{MF}^2 \bar{\sigma} + \lambda_{MF} \bar{\sigma}^3 \stackrel{!}{=} 0. \quad (38)$$

There is always the trivial solution  $\bar{\sigma} = 0$  corresponding to the symmetric phase. At zero density the non trivial solution  $\bar{\sigma}_0 = \sqrt{-m^2/\lambda}$  has a lower energy and represents the spontaneous broken phase. At higher density, the chirally symmetric phase has lower energy. The energy density in the broken phase relative to the symmetric one is

$$\epsilon_0 \equiv \epsilon_{br}(\rho_B = 0) = -\frac{m^4}{4\lambda} = -B, \quad (39)$$

whereby we define  $B$  as a kind of bag constant. It gives the amount of energy density by which the partonic vacuum lies above the constituent quark vacuum. We estimate the sensitivity of the calculation to the input coarse grained potential by comparing the minima of the energy per baryon in both phases. The massless partonic (symmetric) phase has an energy density

$$\epsilon_{sym} = \frac{9}{4} \left(\frac{9\pi^2}{2N_c}\right)^{1/3} \rho_B^{4/3} \quad (40)$$

with a minimum of the normalized energy per baryon

$$\left.\frac{\epsilon_{sym}(\rho_B) - \epsilon_0}{\rho_B}\right|_{min} = 3 \left(\frac{3\pi^2}{2N_c}\right)^{1/4} \left(\frac{m^4}{\lambda}\right)^{1/4} \quad (41)$$

at

$$\rho_{B,sym}^{min} = \frac{1}{3} \left(\frac{2N_c}{3\pi^2}\right)^{1/4} \left(\frac{m^4}{\lambda}\right)^{3/4}. \quad (42)$$

In the constituent quark phase the asymptotic value of the energy per baryon is three times the quark mass:

$$\left.\frac{\epsilon_{br}(\rho) - \epsilon_0}{\rho_B}\right|_{min} = 3g\bar{\sigma}_0. \quad (43)$$

Therefore in order to have a stable broken phase at low density the following condition is necessary (but not sufficient),

$$\left(\frac{3\pi^2\lambda}{2N_c}\right)^{1/4} > g. \quad (44)$$

We note, that with  $g=3.23$  this condition is fulfilled for parameterization (X) but not for (Y). As a result the latter does not have a stable homogeneous phase with broken chiral symmetry.

In the following section we present our numerical results.

## 5 Results in mean field approximation

In this section we discuss the results of the mean field calculations, shown in the figures 5–7, before we compare them with the grid calculation in the next section. In figure 5 we present the energy per baryon as a function of the inverse density relative to the energy of the broken phase at zero baryon density. In the low density limit, the energy per baryon of the broken phase slowly approaches three times the constituent quark mass  $3m_Q = 3g\bar{\sigma}_0$ . This is the preferred state at low densities, where we have a noninteracting dilute system of constituent quarks. Since our coupling constant  $g$ , is fixed from the beginning to yield a constituent quark mass of 300 MeV, the vacuum mass of the “nucleon” is smaller than 938 MeV in both cases (X) and (Y) (cf. table 1). In the chiral limit which we pursue here the nucleon is lighter than the real one. In the upper left corner of both plots the parabola represents the partonic phase.

For the couplings (X) condition (44) is fulfilled, thus the phase diagram may be obtained using the Maxwell construction (dashed line):

For a first order phase transition the equilibrium-condition for a given temperature (in our case  $T = 0$ ) and pressure is

$$G(T, P, N) = \min. \quad (45)$$

In the region of coexistence between the two phases (I/partonic) and (II/constituent quark), the temperature, pressure and chemical potential have to be equal to each other. Hence

$$\mu_B^{I,II} = \frac{1}{N_B}G(T, P, N_B) = \frac{1}{N_B}(F + PV) = \frac{F}{N_B} + P\frac{1}{\rho_B}, \quad (46)$$

where the pressure  $P$  is constant in the coexistence region. At zero temperature the free energy per baryon  $F/N_B$  equals the energy per baryon  $E/N = \varepsilon/\rho_B$  and we can read off from the tangent construction the energy

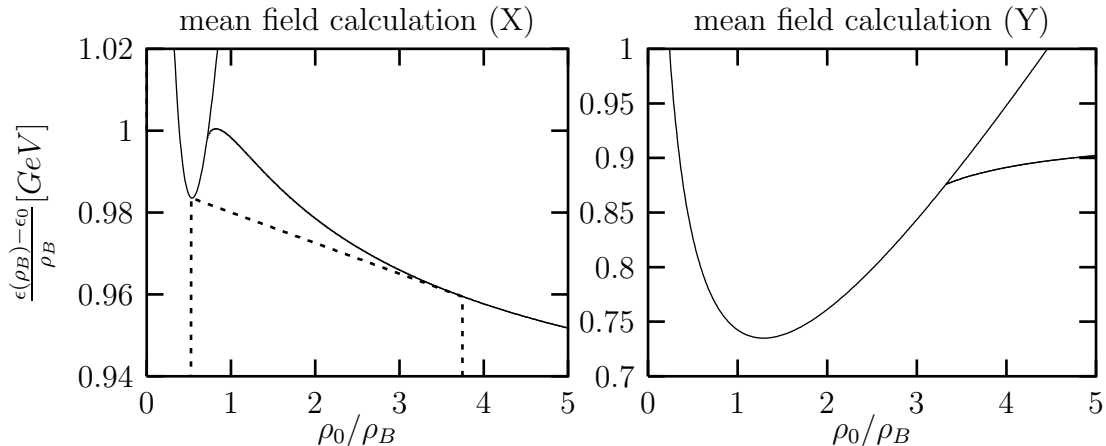


Figure 5: The energy per baryon plotted against  $\rho_B^{-1}$  in units of normal nuclear density  $\rho_0 = 0.16 \text{ fm}^{-3}$  for mean field parameterization  $X$  (left) and  $Y$  (right). Note the different energy scales in the figures. The dashed line in the left plot represents the Maxwell-construction which determines the region of coexistence between broken and chiral symmetric phase.

per baryon as a function of the inverse baryon density in the mixed phase:

$$\frac{E}{N_B} = -P \frac{1}{\rho_B} + \mu_B. \quad (47)$$

The slope is the negative pressure and the intercept with the vertical axis is the baryon chemical potential at the phase transition. The dashed line in figure 5 connects the low density constituent phase with the high density partonic one. The phase transition takes place between 0.27 and 1.90 times normal nuclear density. In between the two phases coexist.

The couplings (Y) do not fulfill condition (44), e.g. we have no stable broken phase. Hence there is no Maxwell construction in this case.

For both parameterizations (X) and (Y) we calculate the pressure from equation (47). The result is shown in figure 6. It shows clearly the stable broken phase for parameterization (X). For parameterization (Y) there is no stable broken phase. At low densities the pressure is always negative,

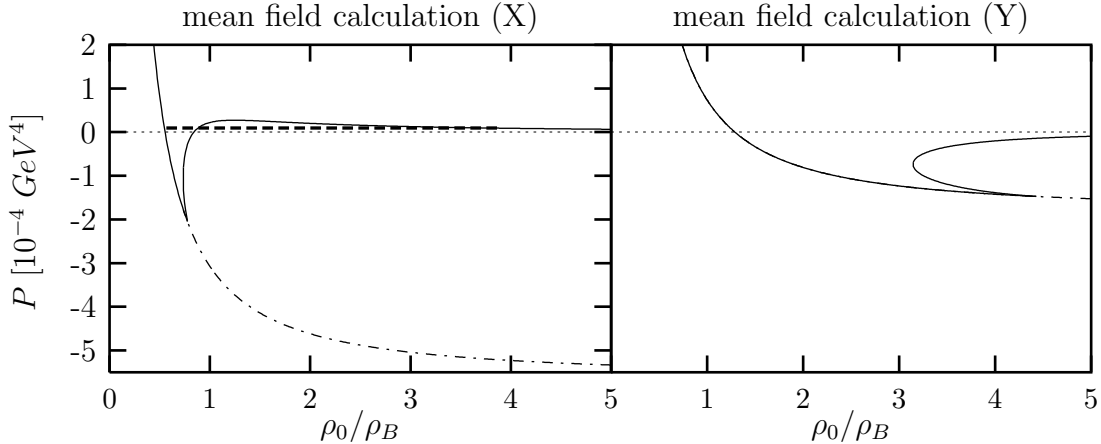


Figure 6: The pressure as a function of inverse baryon density, calculated for mean field parameterizations  $X$  (left) and  $Y$  (right). The thick dashed line in the left plot is the Maxwell-construction. In the case  $Y$  (right) no Maxwell-construction exists. Note that the negative values of the pressure are solutions of the equations but have now physical interpretation. In both cases the pressure for the symmetric phase ( $\bar{\sigma} = 0$ ) asymptotically approaches the bag pressure  $B$  (cf. table 1) for small densities (dashed-dotted line).

thus it is more advantageous to pack the quarks into droplets of massless quarks with nonperturbative vacuum between them than to have loosely bound constituent quarks associated with nucleons.

In figure 7 we present the binding energy per baryon subtracting the “baryon mass”  $3m_Q$ , from the energy per baryon. Note that in the case (X) the system is unbound, the energy of the partonic phase has a minimum at  $\sim 1.8$  times normal nuclear density. This minimum lies on the edge of the coexistence region. In the case of couplings (Y) the system is strongly bound, the minimum of the partonic phase is  $\rho_B = 0.78 \rho_0$ .

The difference between the two cases (X) and (Y) demonstrates that the form of the coarse grained potential  $\Omega$  influences the physics at low momentum scale drastically. In the mean field approximation it is mainly the sigma mass  $m_\sigma^2 = 2\lambda\bar{\sigma}_0^2$  which determines the amount of attraction i.e. bind-

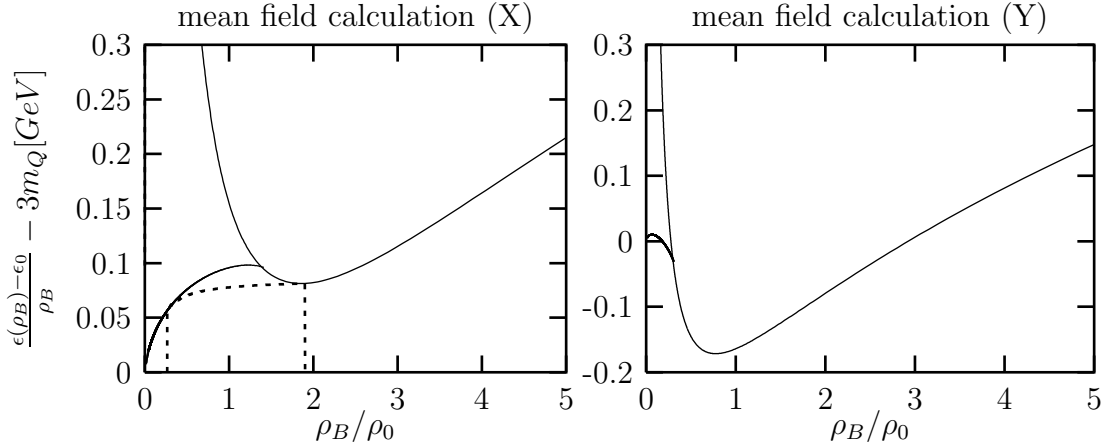


Figure 7: Binding energy per baryon is plotted against  $\rho_B$  in units of normal nuclear density  $\rho_0$ , for the couplings  $X$  (left panel) and  $Y$  (right panel).

ing or unbinding of baryonic matter. Recall the attraction in nonrelativistic Hartree approximation varies as  $-\frac{g^2\rho_s^2}{2m_\sigma^2}$ . Potential (X) with a high  $\sigma$ -mass of 0.728 GeV is less attractive than the potential (Y) with a  $\sigma$ -mass of 0.404 GeV. The meson–meson interaction term  $\lambda$ , also fixes the structure of the intermediate density region. A large  $\lambda$  gives a mixed phase as produced by potential (X) cf. eq. (44). The grid calculation shares the low field strength region with the potential (Y), and has the mass of the  $\sigma$  meson in between of the ones from the potentials (X) and (Y) (see figure 4). Therefore we expect that the equation of state on the grid lies between the extremes determined by the potentials (X) and (Y).

## 6 Comparison of mean field results with grid calculations

In this section we compare the results obtained from the mean field approximations with the ones from the grid calculation. The main results are shown in figures 8 and 9.

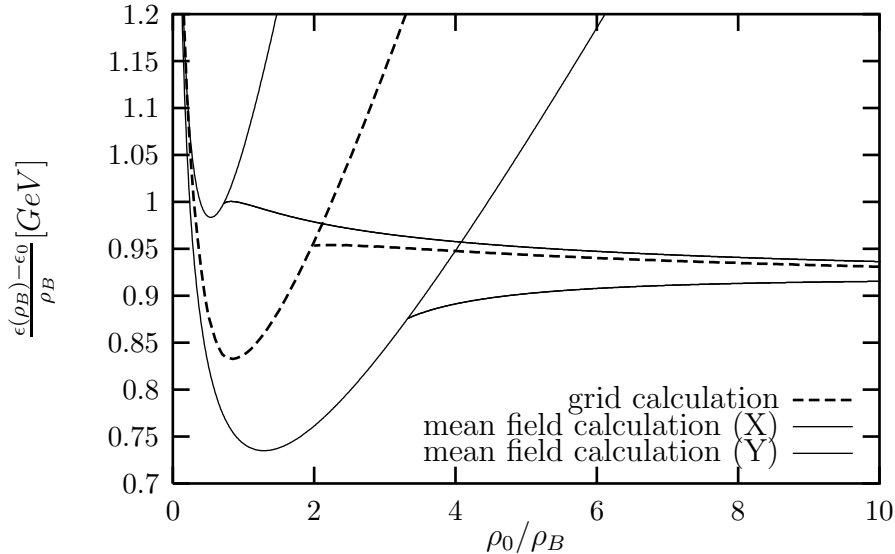


Figure 8: Normalized energy per baryon, calculated on the grid (dashed line) and in the mean field calculations with couplings  $X$  (upper solid curve) and  $Y$  (lower solid curve), is shown as a function of inverse density  $\rho_B^{-1}$ , normalized to normal nuclear density.

In figure 8 we present the energy per baryon obtained in the (X) parameterization of the mean field (upper curve), the (Y) parameterization (lower curve) and the grid calculations (dashed line). The three curves show a very similar behavior. At low density the energy per particle is approaching the same limit of three times the mass of the constituent quarks, as we discussed in the previous section. The nucleon mass is  $\sim 900$  MeV in both cases. With increasing density, one arrives at the point where no broken phase is supported any longer, i.e. the mean field eq. (38) does not have a nontrivial  $\bar{\sigma}$  solution and only the massless partonic phase exists. For the coarse grained couplings (Y), this happens at  $\rho_B = 0.32 \rho_0$ , while for the grid calculation at  $\rho_B = 0.56 \rho_0$ . The parameterization (X) leads to highest transition point at  $\rho_B = 1.32 \rho_0$ . In all three cases the order parameter drops to zero, i.e. we have a first order phase transition.

Since the minimum of the energy per particle in the partonic phase is

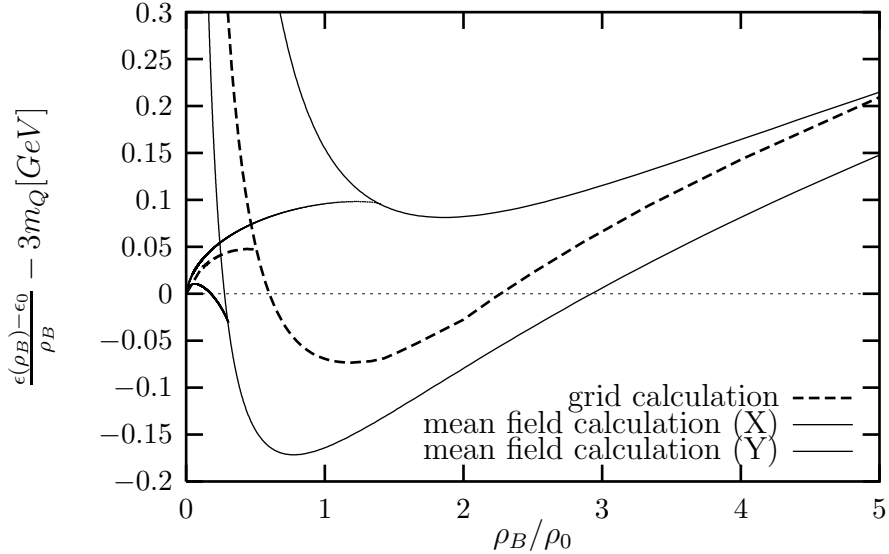


Figure 9: Binding energy per baryon, calculated on the grid and in the mean field approximation with potentials  $X$  (upper curve) and  $Y$  (lower curve), is shown as a function of  $\rho_B$  normalized to normal nuclear density.

below the minimum of the broken phase, no Maxwell-construction is possible and the broken phase is not stable even at lower densities for both the grid calculation and model (Y). This phase starts from zero density and persists until  $\rho_B = 1.17 \rho_0$  for the grid and until  $\rho_B = 0.78 \rho_0$  for the mean field calculation (Y). At these densities the droplets fill up the whole volume. They are bound by  $\approx 74$  MeV (grid) and  $\approx 172$  MeV (mean field), respectively, per baryon number. If one compresses the system above this density the fermi pressure pushes the equation of state higher up in energy.

Contrary to these cases there exists a Maxwell construction for potential (X) as we have seen in the previous section. The region of coexistence between the stable constituent quark phase and the partonic phase ranges from  $0.27 \rho_0$  to  $1.90 \rho_0$ .

In figure 9 we show the equation of state for the three calculations. The coarse-grained couplings (Y) as well as the grid-calculation yield bound sys-

tems. However, in both cases the binding is too strong, 74 MeV per baryon in the grid and 172 MeV per baryon in the mean field calculation with model (Y). The saturation densities lie near normal nuclear density, but baryonic matter is already in a chirally symmetric phase.

## 7 Summary and Conclusion

We have calculated a coarse grained effective potential from renormalization group flow equations in a quark model with explicit meson fields. At the fermi momentum scale we continue the evolution including Pauli blocking. To avoid meson instabilities we switched off the meson loop terms at  $k_{th} \approx k_F$ . The resulting quark matter overbinds and is in a chiral symmetric phase. We presented two mean field approximations to the full grid calculation with different sets of couplings. The grid solution of the flow equation, with the evolution of the meson effective potential omitted below  $k_{th}$ , lies in between the result of these two mean field approximations.

The many body physics found here is very similar to the *NJL* model where one finds a first order phase transition with either a mixed phase or a droplet phase [9]. Also the instanton induced quark interaction of ref. [5] produces a droplet phase of partonic quarks. In the effective potential the determining equation is the relation between the energy per quark in the partonic phase and the constituent quark mass (cf. eqs. (41,43)).

The shape of the droplets in the low density phase have to be determined from an independent calculation including surface effects. The bag produced by the linear sigma model does not confine. It has a finite height, outside the massless quarks acquire a constituent quark mass. Otherwise the solution of the evolution equation is similar to a *MIT* bag type solution with massless quarks inside. Up to now attempts to model the nucleon as a soliton in the linear sigma model have failed due to the instability of the sigma solution arising from the integration over the sea quarks. The evolution equation may be helpful in finding such a soliton solution too.

In our approximation we used lowest order in two cases to address the finite density problem: the coupling constant  $g$ , was fixed during the evolution and the wave function renormalization  $Z$  was set to one. A recent publication of the Wetterich group [11] uses a running meson-quark coupling and obtains a solution with a mixed phase extending from very low to very high



density. In fact the evolution of the coupling constant at finite density is not necessarily the same as at zero density. The equations for the wave function renormalization and the coupling are modified at finite density. Important effects such as pion condensation [17] may appear after the wave function renormalization. One therefore has to make more extended calculations to know the full result for the linear sigma model at finite density.

In quark matter the linear sigma model with only attractive sigma mesons and pions is not sufficient to capture the nuclear physics. Repulsive effects and confinement into nucleons play an important role. To monitor the transition to the deconfined phase one needs an order parameter which keeps track of this transition. Since the linear sigma model with quarks is already a hybrid model, it is not unnatural to include also nucleon degrees of freedom explicitly and trace the transition of nucleon to quark degrees of freedom directly. This has been done in a separate paper [7].

## Acknowledgments

One of the authors (G.P.) would like to thank J. Polonyi for early discussions. This work was supported in part by the US DOE grant DE-FG02-86ER40251 and the Hungarian grant OTKA F026622. T.K. acknowledges DAAD for making his stay in Germany possible. He is also grateful to H.-J. Pirner and C. Wetterich for hosting him during his stay in Heidelberg; he thanks all the members of Institut fuer Theoretische Physik for their warm hospitality to him. This work is partly done during his sabbatical.

## A Calculation of $\partial\Omega^F/\partial k$ and $\partial\Omega^B/\partial k$

In this appendix, we calculate the derivative of the thermodynamical potentials in the heat kernel method.

### The fermionic part of the flow equations:

The fermion part of the thermodynamical potential is written as

$$\Omega^F = N_c N_f I^F(k), \tag{48}$$

with

$$I^F(k) = 2T \sum_{n, \vec{q}} \int_0^\infty \frac{d\tau}{\tau} f(k^2\tau) e^{-\tau[(\nu_n + i\mu)^2 + \vec{q}^2 + g^2\phi^2]}. \quad (49)$$

Using the fact that

$$\frac{df(k^2\tau)}{dk} = -k^5 \tau^3 e^{-k^2\tau}, \quad (50)$$

and putting  $E_{q,k}^2 = g^2\phi^2 + \vec{q}^2 + k^2$ , the derivative  $dI^F/dk$  is evaluated to be

$$\begin{aligned} \frac{\partial I^F}{\partial k} &= -2k^5 T \sum_{n, \vec{q}} \int_0^\infty d\tau \tau^2 e^{-\tau[(\nu_n + i\mu)^2 + E_{q,k}^2]} \\ &= -2k^5 T \left( \frac{d}{dk^2} \right)^2 \sum_{n, \vec{q}} \frac{1}{(\nu_n + i\mu)^2 + E_{q,k}^2}, \\ &= -k^5 T \left( \frac{d}{dk^2} \right)^2 \sum_{\vec{q}} S^F(q, k) \end{aligned} \quad (51)$$

with

$$S^F(q, k) = \sum_n \left[ \frac{1}{(\nu_n + i\mu)^2 + E_{q,k}^2} + \frac{1}{(\nu_n - i\mu)^2 + E_{q,k}^2} \right], \quad (52)$$

where use of the fact has been made in the last equality that the sum w.r.t. the Matsubara frequencies  $\nu_n$  does not change when the sign of the frequencies is changed.

Now the nice point is that the sum in  $S(q, k)$  can be performed analytically, as follows;

$$\begin{aligned} S^F(q, k) &= \frac{d}{dx^2} \sum_n \left[ \ln[(\nu_n + i\mu)^2 + x^2] + \ln[(\nu_n - i\mu)^2 + x^2] \right]_{x=E_{q,k}^2}, \\ &= \frac{d}{dx^2} \sum_n \left[ \ln[\nu_n^2 + (x - \mu)^2] + \ln[\nu_n^2 + (x + \mu)^2] \right]_{x=E_{q,k}^2}. \end{aligned} \quad (53)$$

Then evaluating the derivative, we have

$$S^F(q, k) = \frac{1}{E_{q,k}} \sum_{n=-\infty}^{\infty} \left[ \frac{E_{q,k} - \mu}{\nu_n^2 + (E_{q,k} - \mu)^2} + \frac{E_{q,k} + \mu}{\nu_n^2 + (E_{q,k} + \mu)^2} \right]. \quad (54)$$

Now utilizing the formula

$$\sum_{n=-\infty}^{\infty} \frac{1}{\nu_n^2 + x^2} = \frac{1}{2Tx} \tanh \frac{x}{2T}, \quad (55)$$

we end up with

$$S^F(q, k) = \frac{1}{2TE_{q,k}} \left[ \tanh \frac{E_{q,k} - \mu}{2T} + \tanh \frac{E_{q,k} + \mu}{2T} \right]. \quad (56)$$

Inserting  $S^F(q, k)$  into (51), we have

$$\frac{\partial I^F}{\partial k} = -k^5 \left( \frac{d}{dk^2} \right)^2 \int \frac{d\vec{q}}{(2\pi)^3} \frac{1}{E_{q,k}} \left[ 1 - n(E_{q,k}) - \bar{n}(E_{q,k}) \right], \quad (57)$$

where  $n(x)$  ( $\bar{n}(x)$ ) is the Fermi-Dirac distribution function, respectively

$$n(x) = \frac{1}{e^{(x-\mu)/T} + 1}, \quad \bar{n}(x) = \frac{1}{e^{(x+\mu)/T} + 1}. \quad (58)$$

Now let us calculate the derivative w.r.t.  $k^2$ , which may be put into the integral; since  $k^2$  appears only in the combination  $q^2 + k^2$ , the derivative can be converted to the one w.r.t.  $q^2$ . Then making a partial integration, we obtain

$$\frac{\partial I^F}{\partial k^2} = \frac{k^4}{8\pi^2} \frac{d}{dk^2} \int_0^\infty dq \frac{1}{E_{q,k}} (1 - n(E_{q,k}) - \bar{n}(E_{q,k})). \quad (59)$$

Inserting (59) into (48), we finally reach the formula presented in the text;

$$\frac{\partial \Omega^F}{\partial k^2} = \frac{N_c N_f}{8\pi^2} k^4 \frac{d}{dk^2} \int_0^\infty dq \frac{1}{E_{q,k}} (1 - n(E_{q,k}) - \bar{n}(E_{q,k})). \quad (60)$$

### The bosonic part of the flow equations:

Similarly, with the fermion part, the boson part of the thermodynamical potential involves the integral;

$$\Omega^B(k) = -\frac{T}{2} \sum_{n, \vec{q}} \int_0^\infty \frac{d\tau}{\tau} f(k^2 \tau) e^{-\tau[\omega_n^2 + \vec{q}^2 + m^2]}, \quad (61)$$

with  $\omega_n$  being the Matsubara frequencies for bosons. Here we shall confine ourselves to the case where the boson has no chemical potential. The extension to the case with finite chemical potential is easy.

The derivative w.r.t.  $k$  can be performed as much the same way as the fermion part. The only difference comes in with the formula

$$\sum_{n=-\infty}^{\infty} \frac{1}{\omega_n^2 + x^2} = \frac{1}{2Tx} \coth \frac{x}{2T}. \quad (62)$$

Thus we obtain,

$$\frac{\partial \Omega^B}{\partial k^2} = \frac{k^4}{32\pi^2} \frac{d}{dk^2} \int_0^\infty dq \frac{1}{E_{q,k}} \coth \frac{E_{q,k}}{2T}, \quad (63)$$

with  $E_{q,k}^2 = q^2 + k^2 + m^2$ .

Performing the derivative as before, we have

$$\begin{aligned} \frac{\partial \Omega^B}{\partial k^2} &= \frac{k^4}{64\pi^2} \left[ \frac{1}{m^2 + k^2} \right. \\ &\quad \left. + 2 \int_0^\infty dq \left\{ \frac{1}{E_{q,k}^3} n_B(E_{q,k}) + \frac{1}{TE_{q,k}^2} n_B(E_{q,k})(1 + n_B(E_{q,k})) \right\} \right], \end{aligned} \quad (64)$$

where  $n_B(x)$  is the Bose-Einstein distribution function given by

$$n_B(x) = \frac{1}{e^{x/T} - 1}. \quad (65)$$

Taking the limit  $T \rightarrow 0+$ , we obtain

$$\frac{\partial \Omega^B}{\partial k^2} = \frac{k^4}{64\pi^2} \frac{1}{m^2 + k^2}. \quad (66)$$

## B Connection between the mean field and the flow-eq. result

Let us regard only the density dependent part of the evolution equations (eq. 14). If this part decouples from the meson evolution, we can integrate

this equation analytically:

$$\Omega_{k=0}^F = \int_{k_{initial}}^0 \frac{d\Omega_F}{dk^2} dk^2 \quad (67)$$

$$= \frac{N_c \mu}{8\pi^2} \int_{\mu^2 - g^2 \phi^2}^0 \frac{k^4 dk^2}{(k^2 + g^2 \phi^2) \sqrt{\mu^2 - k^2 - g^2 \phi^2}}. \quad (68)$$

The integral gives the following result:

$$\begin{aligned} \Omega_{k=0}^F = & -\frac{N_c}{8\pi^2} \left( 2\mu^3 \sqrt{\mu^2 - g^2 \phi^2} - 4\mu g^2 \phi^2 \sqrt{\mu^2 - g^2 \phi^2} - \frac{2}{3} \mu \sqrt{\mu^2 - g^2 \phi^2}^3 \right. \\ & \left. + 2(g^2 \phi^2)^2 \log \frac{\mu + \sqrt{\mu^2 - g^2 \phi^2}}{g\phi} \right). \end{aligned} \quad (69)$$

Since one can do the replacements,

$$\begin{aligned} \mu &= \sqrt{k_F^2 + g^2 \phi^2} \\ k_F &= \sqrt{\mu^2 - g^2 \phi^2}, \end{aligned}$$

the potential takes the following form:

$$\begin{aligned} \Omega_{k=0}^F = & \frac{N_c}{4\pi^2} \left( 2k_F \sqrt{k_F^2 + g^2 \phi^2}^3 - g^2 \phi^2 k_F \sqrt{k_F^2 + g^2 \phi^2} \right. \\ & \left. - g^4 \phi^4 \log \frac{\sqrt{k_F^2 + g^2 \phi^2} + k_F}{g\phi} \right) - \frac{N_c}{4\pi^2} \frac{8}{3} \sqrt{k_F^2 + g^2 \phi^2} k_F^3. \end{aligned} \quad (70)$$

Recalling the relation between  $\Omega$  and  $F$

$$\Omega = F - 3\rho_B \mu, \quad (71)$$

we can identify the term in brackets with  $F$ , and this is indeed the fermionic part of our mean field result eq. (36).

We can also do this independent check for the equation (33), but because of the complicated form of our constraint equation this can not be done analytically. Numerical integration of the density dependent part in (33) reproduces again the mean field results.

## References

- [1] B.-J. Schaefer and H.-J. Pirner, Nucl.Phys. **A627** (1997) 481; B.-J. Schaefer and H.-J. Pirner, nucl-th/9903003, to be published in Nucl. Phys. A
- [2] H. G. Dosch, T. Gousset, H. J. Pirner, Phys. Rev. **D57** (1998), 1666
- [3] G. Papp, B.-J. Schaefer, H.-J. Pirner and J. Wambach, hep-ph/9909246
- [4] M. Stephanov, Phys. Rev. Lett. **76** (1996) 4472; R.A. Janik, M.A. Nowak, G. Papp and I. Zahed, Phys. Rev. Lett. **77** (1996) 4876.
- [5] M. Alford, K. Rajagopal and F. Wilczek, Phys. Lett. **B422** (1998) 247;
- [6] J. Berges, K. Rajagopal, Nucl. Phys. **B538** (1999) 215; R. Rapp , T. Schäfer, E. Shuryak and M. Velkovsky, Phys. Rev. Lett. **81** (1998) 53; T.M. Schwarz, S.P. Klevansky and G. Papp, nucl-th/9903048.
- [7] K. Schwenzer, J. Meyer and H. J. Pirner, nucl-th/9908017, submitted to Phys. Lett. B
- [8] S. P. Klevansky, Rev. Mod. Phys. **64** (1992) 649; T. Hatsuda and T. Kunihiro, Phys. Rep. **247** (1994) 221; P. Bozek, Y. B. He and J. Hüfner nucl-th/9806066;
- [9] M. Buballa, Nucl. Phys. **A611** (1996) 393; M. Buballa, M. Oertel, Nucl. Phys. **A642** (1998) 39c, hep-ph/9807422; M. Buballa, M. Oertel, Phys. Lett. **B457** (1999) 261, hep-ph/9810529
- [10] M. Boyce and P.J.S. Watson, Nucl. Phys. **A580** (1994) 500; H.J. Pirner and M. Wachs, Nucl. Phys. **A617** (1997) 395
- [11] J. Berges, D.-U. Jungnickel and C. Wetterich, Phys. Rev. **D59** (1999) 034010; J. Berges, D.-U. Jungnickel and C. Wetterich, hep-ph/9811347 and hep-ph/9811387.
- [12] J. Polchinski, Nucl. Phys. **B231** (1984) 269 J. Plochinski, in Recent Developments in Particle Theory, Proceedings of the 1992 TASI, eds. J. Harvey and J. Polchinski (World Scientific, Singapore, 1993)

- [13] J. Alexandre, V. Branchina and J. Polonyi, Phys. Lett. **B445** (1999) 351.
- [14] R. Shankar, Rev. Mod. Phys. **66** (1994) 129
- [15] E. M. Nyman, M. Rho, Nucl. Phys. **A268** (1976) 408
- [16] L. G. Liu, W. Bentz and A. Arima, Ann. Phys. **194** (1998),387
- [17] H. J. Pirner, K. Yazaki, P. Bonche and M. Rho, Nucl. Phys. **A329** (1979) 491; T. Kunihiro, T. Muto, T. Takatsuka, R. Tamagaki and T. Tatsumi, Prog. Theor. Phys. Suppl. **112** (1993)